Electrospray Gold Standards of Molecular Mass 32- to 52-kDa: Charging Patterns of the Ubiquitous Virus-like Clusters, *I* - $^{197}Au_{144\text{-}5}(SR)_{60}$, *R* = 8 Variants, in Native [HPLC]-ESI-MS

M. Mozammel Hoque, [a*] *David M. Black,* [b] *Laura J. Castellanos-Garcia,* [c] *Yohei Ishida,* [d] *Richard W. Vachet,* [c] *Flavio Maran,* [e,f,g] *Robert L. Whetten* [a*]

[a] *Department of Applied Physics and Material Science, & MIRA, Northern Arizona University, Flagstaff, Arizona 86011, USA.*
[b] *Department of Chemistry, University of Texas at San Antonio, San Antonio, Texas 78249, United States*
[c] *Department of Chemistry, University of Massachusetts, Amherst, Massachusetts 01003, United States*
[d] *Division of Material Science and Engineering, Hokkaido University, Hokkaido 060-8628, Japan*
[e] *Department of Chemistry, University of Padova, Via Marzolo 1, 35131 Padova, Italy.*
[f] *CNR-ICMATE, National Research Council, via Marzolo 1, 35131 Padova, Italy*
[g] *Department of Chemistry, University of Connecticut, 55 North Eagleville Road, Storrs, 06269 Connecticut, USA*

Abstract: Faraday's legendary 'Molecules of Gold' have stimulated intense interest (over 165 years) but have only recently begun to yield their secrets to modern methods of chemical analysis. Here(in), we demonstrate how striking charging patterns emerge directly from native electrospray of large, gold-rich molecules that were generated by reduction of various (8) small gold(I)thiolate complexes [-*RS*-*Au*(*I*)-*SR*-], followed by extensive thermochemical processing to enrich the most robust forms. In each case (*R*), electrospray ionization of a picomolar solution yields a characteristic series of abundant, highly resolved peaks at related (*m/z*)-ratios, that can be used to deduce charges $\{z\ e^+\}$ and hence a distinct molecular mass, $\{M_R\}$. A plot of $\{M_R\}$ versus thiolate-mass $\{m_L\}$ yields a straight line with slope 60.0 (the ligand count) and an intercept of 28,364-*Da*, the mass of 144 Au-atoms. i.e., a unique molecular composition $\{^{197}Au_{144}(SR)_{60}\}$. This formula agrees with the unique chiral-icosahedral structure-model, c@12@42@60@(30,60), the $Pd_{145}(CO)_{60}$-structure, that features a massively-compact globular Au_{114}-core (~1.6-nm) and an intrinsically chiral (*I*) outer shell (~2.0-nm) with *12 distinct ligand types of 5-fold equivalence*], denoted by Martin et al. as 'virus-like' on the basis of its resemblance of icosahedral-virus capsids.

Introduction

Molecular characterization of monolayer-protected clusters commonly known as 'MPCs' is a challenging task. This task often becomes daunting due to strict synthetic procedures, time consuming and laborious, but *crucial*, need for purification and strict solubility parameters required for certain cluster chemistries. Among various available analytical tools for characterization, mass spectrometry has demonstrated great [1–4] as a powerful tool for these synthetic nanostructured molecules.

In nature (geochemistry or microbiology), reduced metallic gold in embryonic form are protected by naturally occurring 'adsorbates' or coordinating ligands {thiolates, cyanides, inter alia}, but the lack of methods and instruments suitable to the investigation of such molecular metallic forms has precluded studies of their intrinsic physicochemical characteristics. This situation motivates the development of such methods and their testing on synthetic analogs of the natural products.

The production of high-quality electrospray ionization mass spectra of monolayer protected clusters (MPCs)[5–12] – a specific type of nanoparticle with core diameters less than approximately 3.0 nm – has generally been limited to hydrophobic[13–17] or to more moderately-sized aqueous varieties. Analysis of aqueous MPCs is a particularly challenging undertaking that requires high quality preparations,[18] significant purification and specific mass spectrometry procedures. Because of this difficulty, examples in the literature of high-quality mass spectra for aqueous MPCs is quite limited. Among the aqueous clusters successfully analyzed to date, the best success has been realized with only a few ligand structures, including, mercaptobenzoic acid,[19,20] glutathione,[21–23] N-acetyl-L-cysteine,[23] sulfonic thiolate,[24] captamine,[25,26] quaternary ammonium,[27] and lipoic acid.[28,29] These and related nanostructures show promise for a range of applications that will benefit from the high-quality mass spectrometry analysis afforded by advances made in instrumentation over the past several decades for large biomolecular components. High resolution, mass accuracy and good signal-to-noise ratio can contribute to unequivocal determination of mass and confident assignment of cluster composition as well as ligand-to-core atom stoichiometry.

This report describes advances in instrumental methodology applied to the identification and quantitative determination of the set of 'critical sizes', i.e. the key species $\{(n, p) = Au_n(\text{-}SR)_p\}$ implicated in the reduction (growth) of gold (Au) metallic clusters in the presence of any of a broad spectrum of thiolate (RS-) ligands. The results obtained are useful in conjunction with other structural deductions, especially the chiral-icosahedral[30] $Pd_{145}(CO)_{60}$-structure of Tran-Powell-Dahl (TPD),[31,32] to draw new physicochemical insights into the natural selection of protected metallic gold clusters.

We have determined parameters and conditions for measurement of two > 50 kDa hydrophilic gold clusters in the gas-phase, along with others readily ionizable compounds in the range of 32-35 *kDa*. We have also demonstrated how the electrospray ionization mass spectrometry (ESI-MS) could be used as a *unique* source for precise identification and composition assignment of ligand-core stoichiometry for discrete metallurgy research. To prove that we have chosen the ubiquitous ~29 kDa (molecular mass) core Au clusters with versatile capping agents/ligands ranging from simplest alkanethiol (C2-C5),[7,14] tertiary amine (captamino),[26] benzyl[32] to more complicated 11-mercaptoundecyl-(tetra) ethylene glycol (ud-TEG-OH)[33] that has been extensively used in biomedical[34–37] and other mass spectrometry applications,[38–40] and 11-mercaptoundecyl)-N,N,N-trimethylammonium hexafluorophosphate (ud-TMA).[27]

The charging patterns are interpreted within this model as characteristic of the *R*-group class. The mass-fraction of the isotopically-pure $^{197}Au_{144}$ ranges from a high 88.6% ($R = C_2H_5$) down to ~60% (PEGylated and quaternized *R*- groups). The remarkable set of features discussed herein suggests that these ubiquitous, robust, virus-like molecules-of-gold may serve an important function as widely available *high-performance standards* for high-resolution metrology, a goal that stipulates specific benchmarks for further development and extensions.

Experimental section

Synthesis

The synthesis of ~50 kDa ud-TEG-OH/ Au, ud-TMA / Au, C2-C5, benzyl, and captamino (see **Figure 1** for molecular structure) gold clusters are described elsewhere. [See the **Table 1** for references].

Methods

The HPLC-MS methods for ~50 *kDa* ud-TEG-OH/ Au, ud-TMA / Au are described below. For the case of other ligands, see the articles where they have been described previously (Table 1 for the reference articles).

HPLC-UV-MS method conditions

Liquid chromatography (LC) experiments were performed on an Eksigent nanoLC 2D system coupled to a Bruker micrOTOF time-of-flight mass spectrometer (MS). All separations were carried out using an Ace 300 Å C18 HPLC column (0.5 mm x 150 mm, 3 µm particle size) (Advanced Chromatography Technologies Limited, Aberdeen, UK) maintained at ambient laboratory temperature. LC and MS conditions were specific to the systems analyzed. For the gold / (11-mercaptoundecyl) - (tetra) ethylene glycol preparation,[33] reversed phase LC was employed with water (mobile phase A) and methanol (mobile phase B) and no additional mobile phase modifier. For the gold / (11-mercaptoundecyl)-N, N, N-trimethylammonium hexafluorophosphate preparation reversed phase chromatography with ion-pairing was employed. Mobile phases were water (mobile phase A) and acetonitrile (mobile phase B) each containing 0.1% formic acid. In each case, a linear gradient method was used for separation of the components of the sample for subsequent sample introduction to the mass spectrometer. In both cases the proportion of mobile phase B was varied from 5% to 100% over 20 minutes.

The gradient was immediately followed by a 5-minute hold at 100% MP B and a subsequent re-equilibration to initial method conditions for 15 minutes. A 10 µL/min flow rate was used for all experiments. Injections – 5.0 µL – were carried out by an Eksigent AS-1 autosampler configured with a 20-µL sample loop. All solvents for direct infusion and LC-MS were obtained from Fisher Scientific (Fairlawn, NJ).

Mass spectrometer acquisition settings were selected to acquire data from *m/z* 100 - 10,000, and 10,000 spectra were summed to yield the displayed spectra. Mass spectrometer parameters for the ud-TEG-OH/ Au system were as follows: (1) nitrogen drying gas temperature, 350 ºC; (2) nitrogen dry gas flow rate, 3 L/min, (3) capillary voltage, 4 kV, (4) end plate offset, -500 V, (5) nebulizer, 1.4 bar, (6) capillary exit, 100 V; (7) skimmer 1, 33 V; (8) hexapole rf, 800 V; (9) lens1 transfer time, 100 µs; and (10) lens 1 pre-pulse storage time, 33 µs.

For the *ud-TMA / Au* system, these parameters were altered as follows: (1) nitrogen drying gas temperature, 250 ºC; (2) nitrogen dry gas flow rate, 4 L/min, (3) capillary voltage, 4.5 kV, (4) end plate offset, -500 V, (5) nebulizer, 0.5 bar, (6) capillary exit, 150 V; (7) skimmer 1, 33 V; (8) hexapole rf, 800 V; (9) lens1 transfer time, 88 µs; and (10) lens 1 pre-pulse storage time, 27 µs.

In the case of ESI-MS analysis of C2-5/Au (see **Figure 2** for C2 and C3), a Bruker Maxis impact II instrument is used, and the dilution factor was 1:30 (molar concentration of 1 mg/mL) returning the total sample consumption of ~500 ng or 0.5 µg, which yields ~15 picomol. So, the instrument thus achieved *sub-picomol* sensitivity.

The instrument acquisition parameters of Maxis impact II (Q-TOF) are provided in our earlier work.[14] For the case of Benzyl/Au and cocktail sample analyses, a Bruker Maxis impact (separate instrument, earlier version of Maxis impact) was used, and the acquisition parameters are as follows:

ESI-MS. Electrospray ionization mass spectra are acquired in the positive-ion mode, with the mass-range typically set for m/z 1,000−20,000 for Benzyl/Au system, and 6,000-14,000 for cocktail sample.

Source: Nebulizer 0.4 Bar, Focus: Active, Capillary: 4.5 kV, Dry Heater: 220 °C, End Plate Offset: -500 V, Dry Gas: 4.0 l/min, Charging Voltage: 2000 V. *Quadruple*: Ion Energy (MS only): 5.0 eV, Isolation Mass (MS only): *m/z* 1500/800.00, Collision Energy: 8 eV, Collision Cell RF: 2000.0/1200 Vpp, Set Transfer time 120/74 µs, Set PrePulseStorage time 55/25 µs. *TOF*: Corrector Fill: 57.2 V, Corrector Extract: 665.3 V, Corrector Lens: 6055.4 V, Reflector: 2750.0 V Decelerator: 721.8 V, Flight Tube: 9.9 kV, Detector TOF: 1827.6 V.

Results and discussion

Typically, the desired gold-rich molecules may be generated efficiently in high yield by chemical reduction of aureus Au(*I*) thiolate precursors, i.e. oligomeric (-Au(*I*)-S(R)-)x, which are prepared *in situ* by the reaction of auric salts and the respective thiols, stoichiometrically

$$\text{Au}(III) + 3\ \text{RS-} \rightarrow \text{“Au}(I)\text{-S(R)”} + \text{RS-SR}.$$

The reduction products are invariably strongly colored, whereas non-metallic byproducts are colorless. Various post-reduction procedures are used to remove such byproducts, and thereby obtain high-carat molecular substances in solid-state (powder) form or in true solutions (solvents matched to the R-group

characteristics). Potentially, there is enormous variety arising from the definite compositions or 'sizes' {*n, p*} obtained for each selection of R-group.

Accordingly, the mixture of products obtained are characterized by various analytical and spectroscopic, diffraction and microscopy methods that, despite their undisputed special powers, are typically unsuited to the quantitative and complete precise determination of the {*n, p*} (*Au, SR*) compositions of all major gold-rich products in the solution. However, the method of native electrospray mass spectrometry (ESI-MS), performed directly on these dilute solutions, offers a route to the determinations.

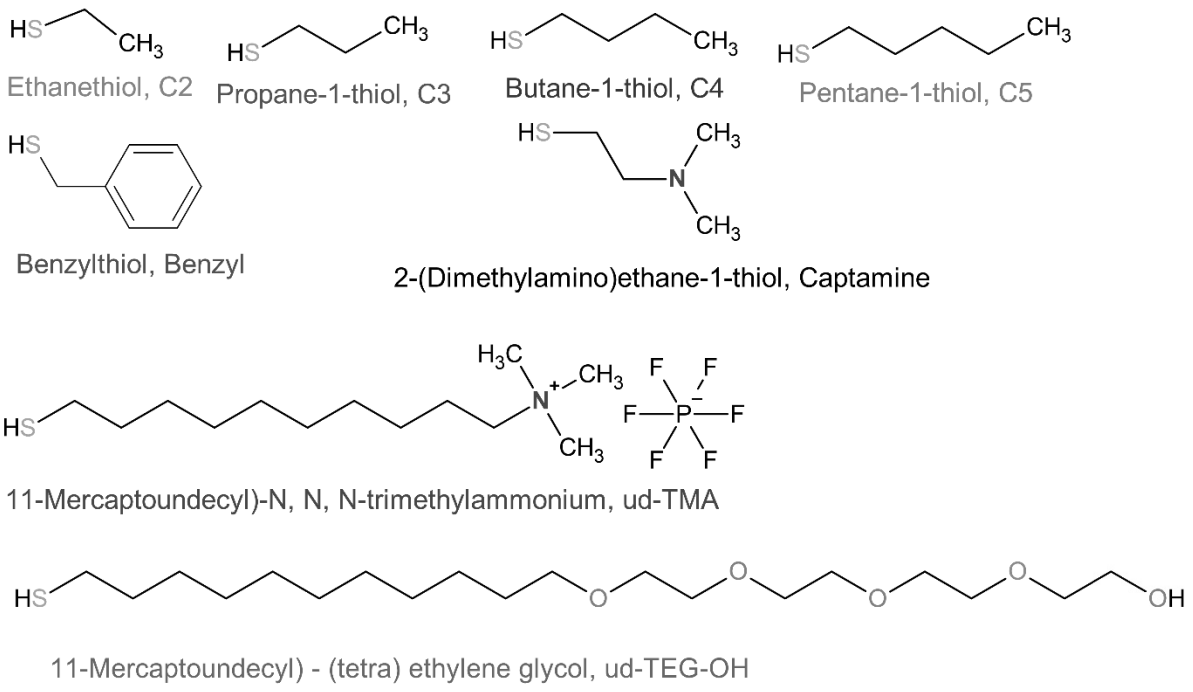

Figure 1: Molecular structure of eight differents ligands used to capped Au clusters in this work.

Figure 1 illustrates the molecular structure of the eight ligands, ranging from ~61 to 400 Da, that are used as a capping agent for the Au metal core of ~29 kDa that are discussed in this work. We can determine the charge state from the isotopic pattern due to the instrumental high-resolution capability as shown in **Figure 2**. The peak-to-peak *m/z* difference is 0.25 *Th*; [here *Th* (Thomson) is the unit of *m/z*] (**Figure 2,** top frame), which confirms the charge state 4^+. The same should be true for charge state 3^+ as shown elsewhere,[14] where the peak-to-peak *m/z* difference is 0.33 *Th*.

Figures 2 and **3** display a collection of typical electrospray mass spectra for the respective samples, i.e., the raw (unprocessed) results of the ESI-MS analyses of highly diluted solutions of the reaction products.

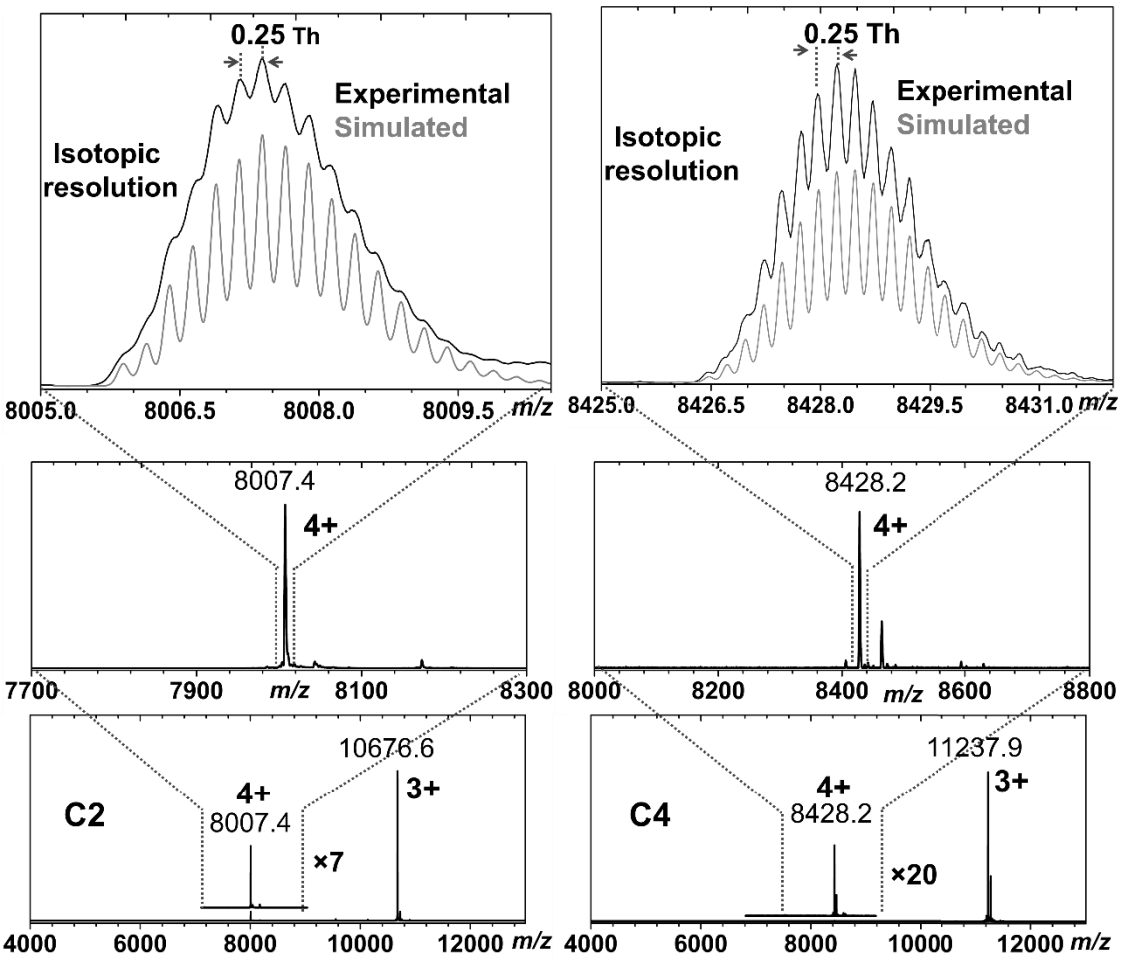

Figure 2: Isotopic pattern of alkane-thiolated Au clusters (mass ~34 kDa) for charge state confirmation. The bottom panel shows the original mass spectra in the range of *m/z* 4000-13000 for charge states 3^+ (dominant) and 4^+. The abundance of the charge state 4^+ for both cases (C4, left panel; C2, right panel) are intentionally enhanced (as mentioned in the Figures) for better visual inspection. The middle section shows the magnified version of the charge state 4^+, whereas the top part demonstrates the isotopic pattern (peak to peak *m/z* difference 0.25 *Th*) along with the relevant simulated pattern as noted in the Figures.

Each mass spectrum is dominated by a series of sharp peaks, i.e., occurring at definite values of *m/z*, which depending on the sample lie within the range of several thousand to well over ten thousand Th: specifically, from *m/z* ~ 3.5 to 19k and beyond (not shown) to ~ 40k. Such mass spectra are suggestive of a long series of discrete compounds or components of the reaction-product mixture. The picture obtained is really quite complex. Certain samples (R-groups) give a closely spaced series in the lower (*m/z*)-range, while others give a widely spaced series, or even a single dominant peak, at much higher (*m/z*)-value(s).

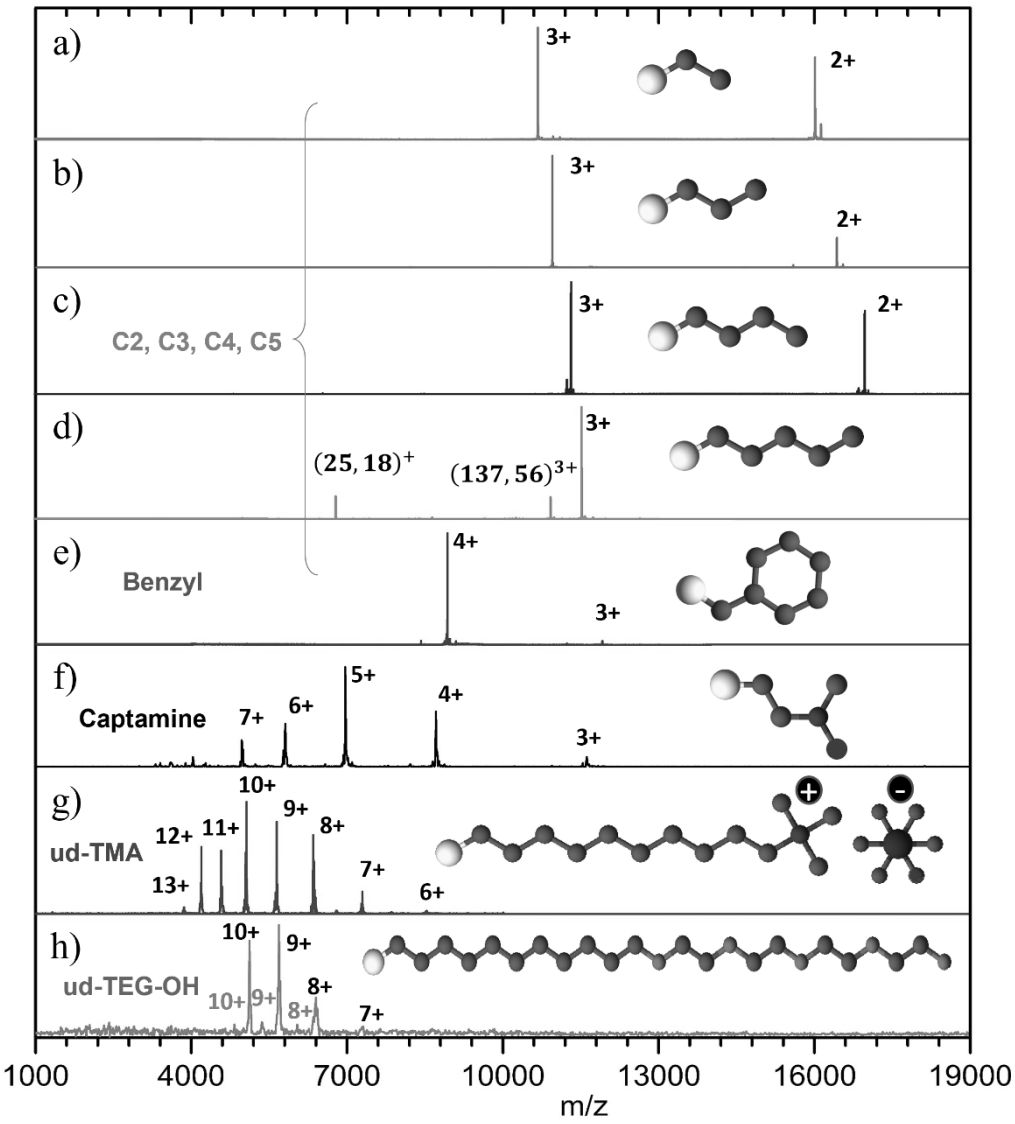

Figure 3: Positive ion mode ESI-MS of different thiolated (-RS) 29 kDa (core) Au_{144} gold clusters in the range of *m/z* 1,000-20,000 with different charge states. Top four traces are alkane thiolated SC2 [red, (a)], SC3 [green, (b)],[7] SC4 [navy blue, (c)], and SC5 [purple, (d)].[14] The bottom four traces are aromatic thiolated benzyl [wine, (e)],[32] tertiary amine thiolated [black, (f)],[26] quaternary ammonium-PF_6 [blue, (g)],[27] and tetra-ethylene glycol, ud-TEG-OH [gold, (h)].[33] For LC traces of ud-TMA (g) and ud-TEG-OH (h) see **Supplementary Figure S1**.

The mass spectra shown in **Figures 3 and 4** (h) were obtained via LC-MS analysis of the ud-*TEG-OH/Au* nanocluster preparation. A combination of water and methanol mobile phases, necessarily with no added mobile phase modifier or electrolyte, provided the necessary conditions for ionization. It is possible that the addition of a mobile phase modifier inhibits ionization due to the detrimental effect that increased ionic strength has on electrospray ionization signal of weakly ionizing compounds, in general. Further investigation is warranted.

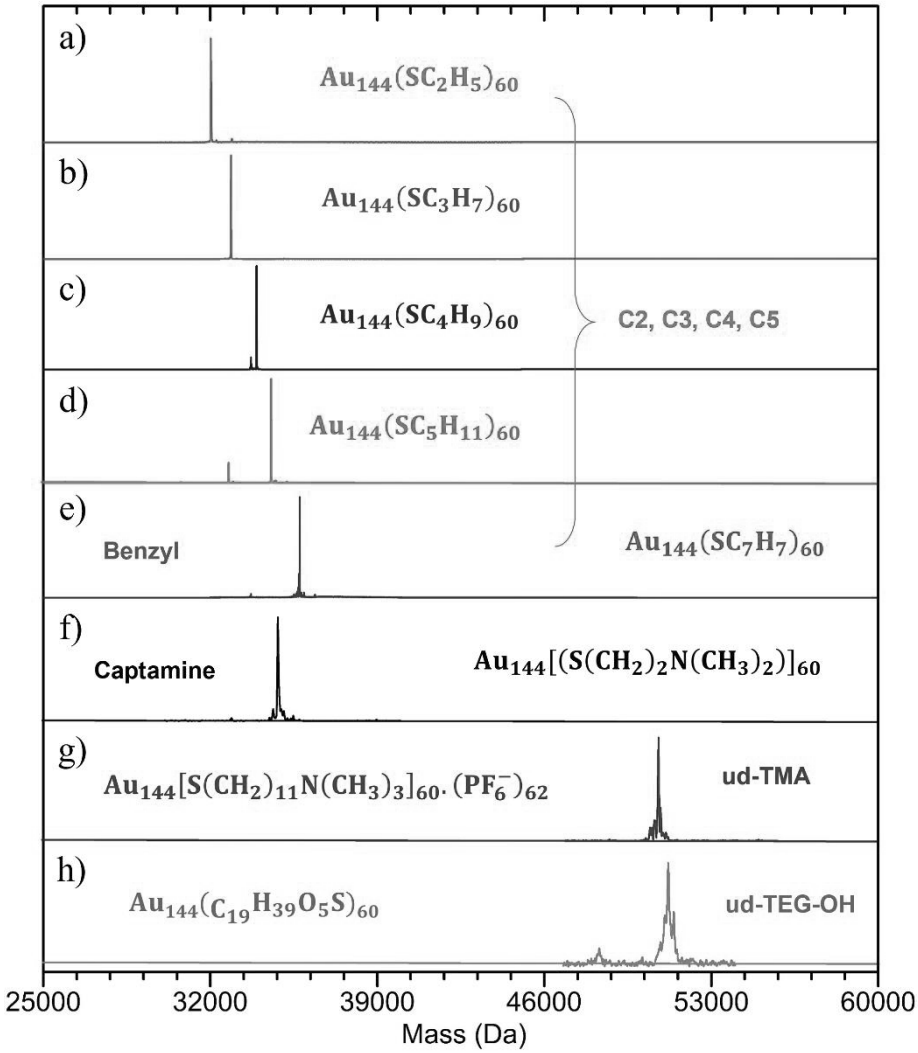

Figure 4: The mass spectrum for each sample in **Figure 3** are replotted on a (molecular) mass (*m*) scale in the range of 25-60 kDa, via multiplication of the (*m/z*)-scale by the identified dominant (assigned) *z*-values; for the deconvoluted unit mass (see **Supplementary Figure S2**). Thiolate dependent mass shift of the unique core ~29 kDa (Au_{144}) are observed: alkane thiolated in the range of 32-35 kDa [top four traces, (a-d)], benzyl 35 kDa [wine, (e)], captamino 34.8 kDa [black, (f)], quaternary ammonium [blue, (g)], and ud-TEG-OH [gold, (h)] ~50 kDa.

To achieve the best ESI signal strength, a high nitrogen gas-temperature, 350 ℃, was employed. Presumably this assisted evaporation of water and methanol solvent molecules from the more hydrophilic portions of the cluster. The ionization difficulty of the more hydrophilic nanoclusters may be related to the ethylene glycol region of the protecting ligands and the highly favorable interaction with water molecules (i.e., hygroscopic/hydrophilic) and solution cations such as sodium ions. Tetra ethylene glycol units are known to bind sodium ions well.[41]

In the spectrum shown in **Figure 3** (h) the distribution having the highest signal strength ranges from 7^+ to 11^+, with 9^+ being the most abundant. The intact mass determined from the sequence of higher abundance charge states is consistent with a {*n*, *p*; 144, 60} cluster, (where *n*, *p* represent the number of Au atoms and thiols, respectively). The total mass of the cluster was calculated using the ligand composition – $C_{19}H_{39}O_5S$ – in the proportion 144:60, gold: ligand. Because the ligand chemistry on this cluster is neutral (i.e., neither acidic, basic, nor ionic), the charge on each of the ions is likely determined by the number of bound protons and / or alkali metal cations, plus contributions from any inherent charge on the cluster. It is possible that multiple ligands may be involved in hydrogen bonding of protons in solution and these interactions are maintained during the electrospray process. The ability to measure intact MPCs is very valuable and will be utilized in future studies to estimate conformational and/or ligand distribution uniformity for homogenous and mixed-monolayer protected clusters.

The mass spectra shown in **Figures 3 and 4** (g) were obtained from LC-MS analysis of the *ud-TMA/Au* preparation. Ionization of this sample also benefited from the use of liquid chromatography for sample introduction to the mass spectrometer to assist with separation of salts and other molecules from the more difficult-to-ionize cluster components. Because the ligand chemistry of this preparation is significantly different than the ud-*TEG-OH* variant, altered ionization conditions were employed. Here, a combination of water and acetonitrile mobile phases, each containing 0.1% formic acid was chosen for analysis. The intrinsic charge from the quaternary ammonium group requires a specifically chosen counter ion for successful synthesis of these clusters. In this case, hexafluorophosphate (PF_6^-) was used, making these clusters more soluble in acetonitrile and other organic solvents. Accordingly, the solvents used for LC and MS sample introduction were chosen in hopes of solvating the cluster, while allowing for control of retention and elution from the C18 column by selection of miscible solvents. Formic acid was added to both mobile phases at 0.1%, in similar fashion to what might be employed for LC-MS of small molecule quaternary ammonium compounds in an effort to replace non-volatile PF_6^- anions with formate.

In the case of ud-TMA/Au shown in **Figure 3** (g), the ESI-MS analysis reveals a single charge-state distribution is detected ranging from 6^+ to 13^+, with 9^+ being the most abundant. The intact mass determined from the sequence of higher abundance charge states is consistent with [144, 60]. In this case, the total mass of the cluster was calculated using the ligand composition – $S(CH_2)_{11}N(CH_3)_3.PF_6^-$ in the proportion

144:60, gold: ligand. For this ligand chemistry, protonation is not the source of charging during the ESI process. Instead, the range of charge states observed is determined by the number of ligands (ud-TMA) that remain PF_6-unmatched (unpaired), upon ESI-charging (volatilization) of the cluster. This mass spectrum, along with the chromatographic trace, indicates that the terminal quaternary ammonium functionalities maintained the corresponding PF_6^- counter ions during the chromatographic separation. No difference in retention time was observed for the precursor ion populations of different charges (**Supplementary Figure S1**). Upon ionization, some PF_6^- counterions are separated from the cluster, resulting in this distribution of charge states observed. Here, again, it is possible that more than one gas-phase conformation may exist for this cluster species and that for some of those multiple ligands interact with any given PF_6^- counter ion. As is the case with the ud-TEG-OH protected cluster, the ability to measure intact MPCs is very valuable and will be utilized to determine ligand distribution uniformity for homogenous and mixed-monolayer protected clusters (ligand place-exchange and bioconjugation).

Table 1: The predominant ligand dependent molecular masses of the ubiquitous clusters $Au_{144}(\text{-SR})_{60}$ discussed in this article.

No. of Samples	Ligand formula	Code name	Solvents	Electrolyte & LC/DI	Ligand mass, m_L (Da)	Exp. molecular mass, M_R (Da)	Calculated Molecular mass (Da)	Difference (Da)	Organic molecular mass (Da)	Ref.
1	SC_2H_5	C2	DCM	None/DI	61.0	32023.9	32029.9	+6.0	3665.9	7
2	SC_3H_7	C3	DCM	None/DI	75.0	32864.8	32871.8	+7.0	4507.8	7
3	SC_4H_9	C4	DCM	None/DI	89.0	33705.7	33712.7	+7.0	5348.7	14
4	SC_5H_9	C5	DCM	None/DI	103.1	34546.7	34555.5	+8.8	6191.5	14
5	SC_7H_9	Benzyl	DCM/ ACN	TFA/DI	123.0	35744.8	35754.9	+10.1	7390.9	32
6	$S(CH_2)_2N(CH_3)_2$	Captamine	DCM/ ACN	HFIP/DI	105.1	34838.4	34811.4	-27.0	6447.4	26
7	$S(CH_2)_{11}N(CH_3)_3 \cdot PF_6^-$	udTMA	H_2O	Formic acid/LC-MS	390.2	52064.0	52079.0	+15.0	23224.1	27
8	$C_{19}H_{39}O_5S$	ud-TEG-OH	H_2O	None/LC-MS	379.3	51118.3	51137.7	+19.4	22773.7	33

Abbreviations: DCM: dichloromethane, ACN: acetonitrile, DI: direct infusion, TFA: trifluoro acetic acid, HFIP: hexafluoro isopropanol

One might reasonably conclude that there is a vast plurality of molecular masses, and hence compositions {*n, p*}, for any given sample (R-group), and that each set {*n, p*} is likely unrelated to the set {n', p'} of compositions present in any other sample (*R*'-group). However, close inspection of the set of {m/z} values measured for the dominant series observed in each case reveals a simple arithmetic relation, suggesting that these ions arise from a series of integer charge-states {z} associated to a common molecular mass m = M_R, characteristic of each sample (ligand identifier R). Similar phenomena in electrospray of

certain large biomolecules, e.g., globular proteins / enzymes[42–45] and oligonucleotides, are well established and understood as (de)protonation series. We have demonstrated the confirmation, in several cases, of the charge assignment, using spectra obtained at 'isotopic resolution', i.e., 1 Da spacings at up to ~ 40-kDa.

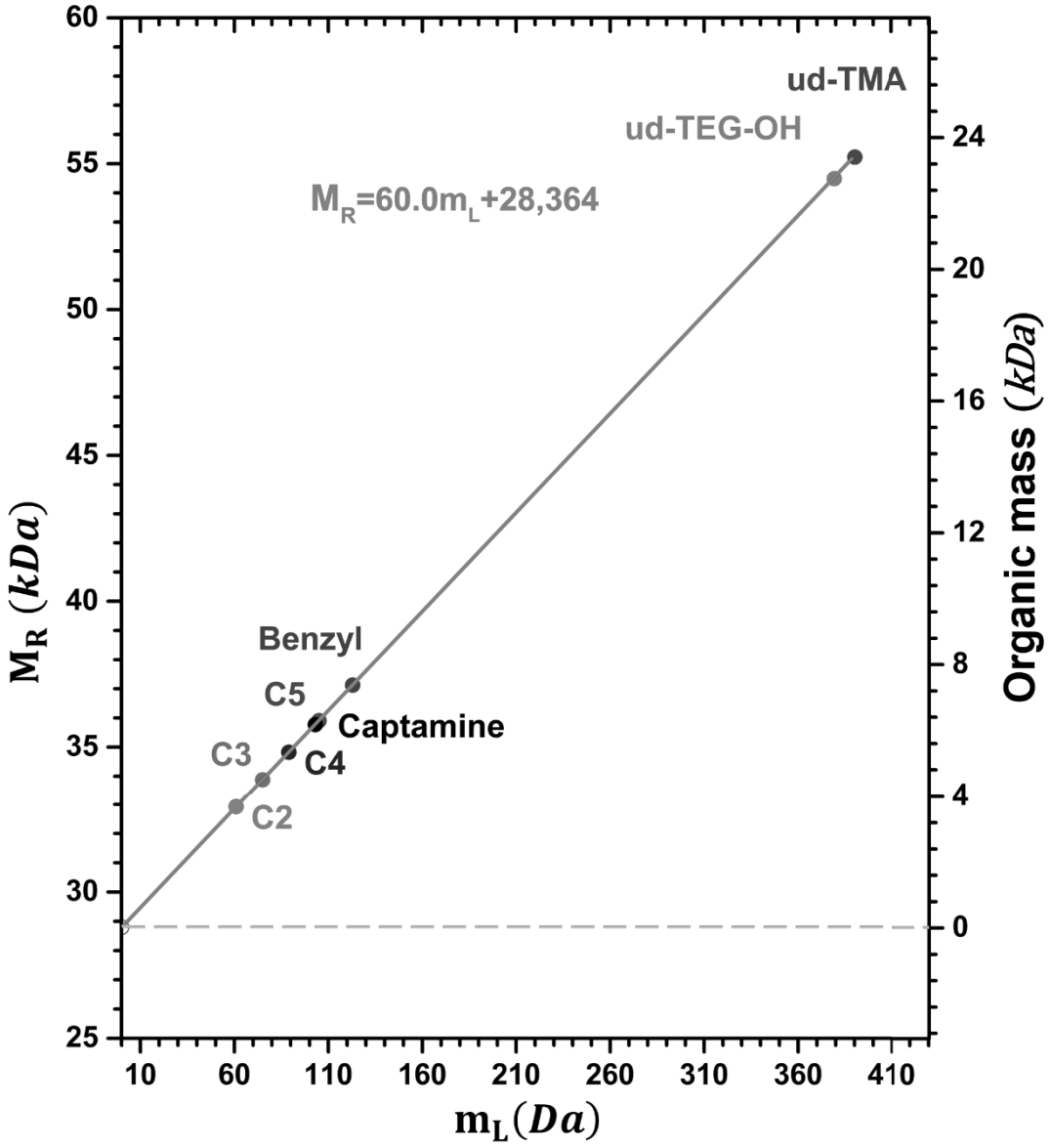

Figure 5: Graphical analysis of the total masses {M_R} versus the respective ligand masses {m_L} for respective Au clusters.

Accordingly, in **Figure 3**, the dominant series is labeled by the identified (assigned) charge labels, z = 1, 2, 3, … *z*-max. Also, in **Figure 4** the *z*-specific regions in the mass spectrum for each sample are

reproduced on a (molecular) mass (m) scale, via multiplication of the (*m/z*)-scale by the identified (assigned) *z*-values.

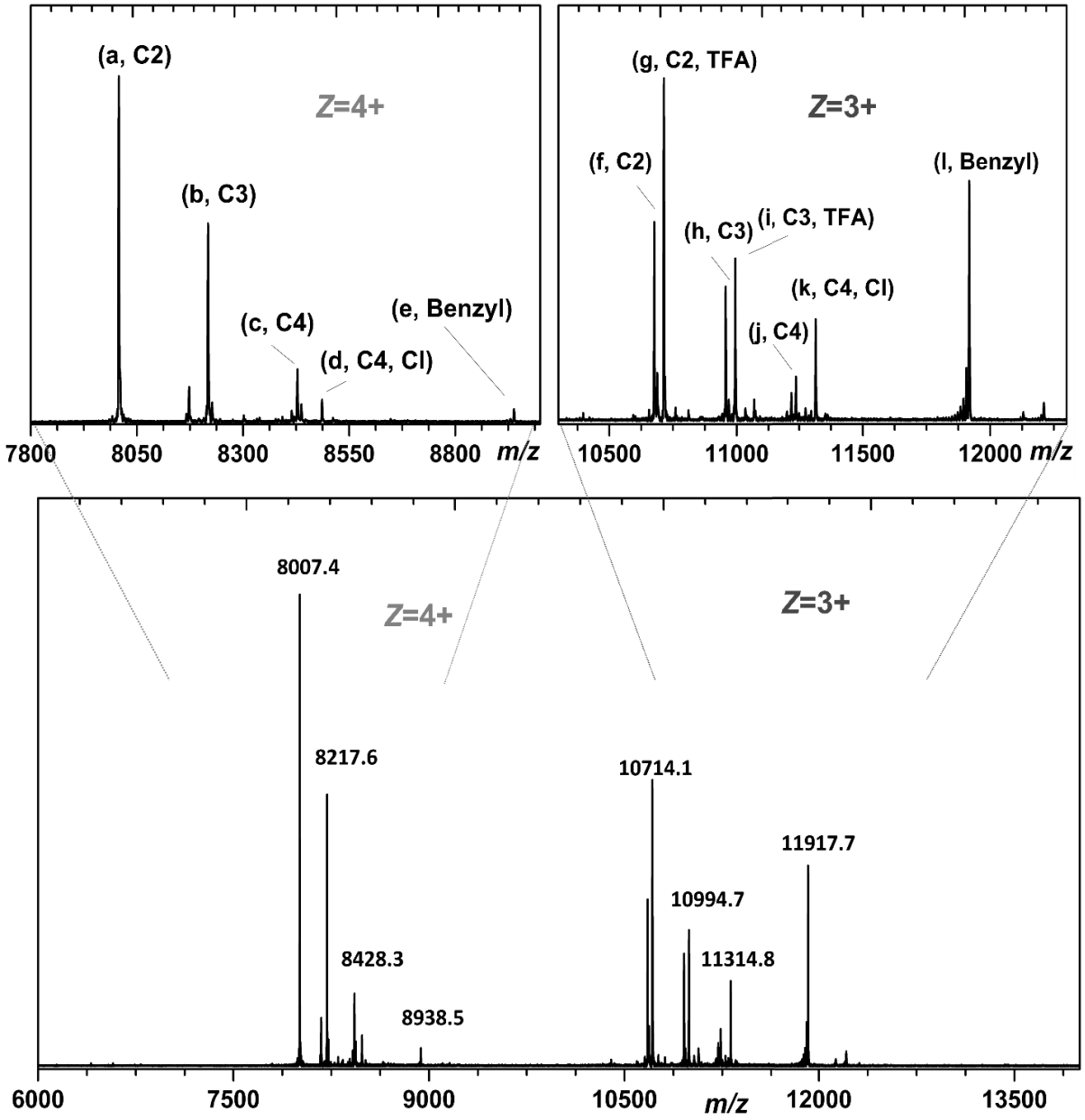

Figure 6: Mixture of C2-C4 and Benzyl-capped Au clusters with an inset showing the expanded version of charge state 3^+ (right side) and 4^+ (left side). For the peak assignments see **Table** 2.

Figure 3 shows how the integer (*z*) multiplication of the (*m/z*) scale brings each series into precise alignment at a single, well defined total molecular mass, M, specific to each sample (ligand) selected. These

predominant molecular masses are collected into **Table 1** and are plotted in **Figure 5** vs. a key ligand characteristic.

Table 2: Peak assignments of **Figure 6**.

Peak	Assignment	Charge (z+)	*m/z* (observed)	*m/z* (calculated)	*m/z* (difference)
a	$Au_{144}(SC_2H_5)_{60}$	**4**	8007.4	8007.5	+0.1
b	$Au_{144}(SC_3H_7)_{60}$	**4**	8217.6	8217.8	+0.2
c	$Au_{144}(SC_4H_9)_{60}$	**4**	8428.4	8428.2	-0.8
d	$Au_{145}(SC_4H_9)_{60} - Cl$	**4**	8486.2	8486.4	+0.2
e	$Au_{144}(SC_7H_7)_{60}$	**4**	8938.5	8938.5	0.0
f	$Au_{144}(SC_2H_5)_{60}$	**3**	10676.5	10676.6	+0.1
g	$Au_{144}(SC_2H_5)_{60} - TFA$	**3**	10714.1	10714.3	+0.2
h	$Au_{144}(SC_3H_7)_{60}$	**3**	10956.9	10957.3	+0.4
i	$Au_{144}(SC_3H_7)_{60} - TFA$	**3**	10994.7	10994.9	+0.2
j	$Au_{144}(SC_4H_9)_{60}$	**3**	11237.4	11237.6	+0.2
k	$Au_{145}(SC_4H_9)_{60} - Cl$	**3**	11314.8	11315.2	+0.4
l	$Au_{144}(SC_7H_7)_{60}$	**3**	11917.7	11917.9	+0.2

Clearly these results are compatible with a distinct, dominant (*) compound, of unknown composition (n, p)*, for each sample / ligand R-group selected. Note also from **Figure 2** that these determined molecular masses range from ~ 32-kDa to above ~ 52-kDa, or roughly 42 ± 10 kDa. For convenience of reference, the mass of a single Au-atom, m_{Au}, is ~197 Da or roughly 0.2-kDa.

Therefore, multiplying these numbers (in kDa) by ~ 5 gives an estimate of the total mass in Au-atom equivalents: 210 ± 50 Au atoms. These numbers are well into the range where (unprotected) gold (Au) clusters can assume the essential crystallographic forms of the corresponding bulk phase(s), as they correspond to a nano-crystallite of equivalent diameter ~ 1.7 - 2.2 nm. Because the distance d_{111} separating close-packed (111) lattice planes in *FCC*-Au is only 0.235-nm, this implies seven-nine lattice planes along each crystallographic [111] axis, easily sufficient to define a structure-type. However, the total mass of the ligands (++) is omitted from this discussion, and it is not negligible.

In fact, referring to the ligand molecular masses in **Table** 1, one notices a striking correlation between the set of (known) ligand masses, $\{m_L\}$, and the set of total molecular masses, $\{M_R\}$. **Figure 5** presents a graphical analysis of this correlation in a plot of the total masses $\{M_R\}$ versus the respective ligand masses $\{m_L\}$. A linear expression may be fit to these data-points, extrapolating to an intercept (limit of zero ligand-

mass m_L) at 28,364 Da, and a value of 60.0 for the slope. The simple interpretation of this correlation is: (i) these are indeed binary* compounds (Au, SR) in which there is a unique total (M_{Au}) of 28,364-Da; (ii) dividing by the mass per Au atom, i.e. m_{Au} = 197 Da, gives 144.0 Au atoms, provides a number (144*) common to all the respective substances (ligand R-group identities); and (iii) the ligand (*RS*-) count is 60 in every case, i.e., the residual (intercept) indicates that the total mass of ligands (M_R - 28,364), which is divided by the mass per ligand.

We thus conclude that the apparent complexity of **Figures 3** and **4** reflects but a *single, unique* special composition (144-5, 60) common to all experimental (synthetic) preparations. With this core conclusion firmly in place, all minor peaks can readily be accounted for in a similar fashion, either as byproduct (n, p) compositions or as adducts (electrolyte, solvent etc.) of the main (144,60) composition. **Figure 6** gives confirmatory evidence of charge-state determinations and isotopic abundances and of the comparative (internal) analysis of 'cocktails' (**Figure 6**) produced by mixing of certain sets of samples. Evidently, inter-cluster reactions are not significant under the conditions employed herein, as the main spectral features are assigned without invoking ligand-exchange processes.

This investigation, employing modern ESI-MS instrumentation and procedures, establishes the following:

(1) The dominant final products of the completed reactions are binary compounds consisting of Au and SR, with negligible amounts of other compounds.

(2) These binary compounds have definite molecular masses and compositions, which may be invariant over a wide range with respect to different ligand types, although there may be some steric exemptions.

(3) The high yield and dominance of these binary compounds suggest that they are ubiquitous and demand a unique explanation for their physicochemical origins.

To explain this phenomenon, one possibility is that the formation of the binary compounds is driven by thermodynamic stability. The Au-SR bond may be highly stable, leading to the formation of these binary compounds as the most energetically favorable products. Another possibility is that the formation of these binary compounds is controlled by kinetic factors, such as the rate of ligand exchange or the accessibility of certain sites on the Au surface. Additional research may be needed to determine the most likely explanation for this phenomenon.

Acknowledgements

The authors thank Tiziano Dainese from the University of Padova, Italy for providing C2-C5 and Benzyl samples. We would like to thank Mr. Blake Rogers for his assistance in the ESI-MS instrumentation help, and Mrs. Nahida Akter Seema for her assistance in preparing ESI-MS sample preparation.

The authors would like to acknowledge support from the Welch-Foundation Grant AX-1857; "Fundamental Chemical Research on Larger Molecular Noble-Metal Clusters". L.J.C. and R.W.V. acknowledge funding from the National Science Foundation Grant CHE-2108044.

Author information

Contributions

The manuscript was written through contributions of all authors. All authors have given approval to the final version of the manuscript.

Corresponding Authors

*Robert L Whetten (robert.whetten@nau.edu) and *M. Mozammel Hoque (mohammad.hoque@nau.edu)

Competing interests

All authors declare no competing interests.

Additional information

Supplementary information

The online version contains supplementary material available at on the nature publications website and includes the supplementary Figures.

References:

(1) Chakraborty, P.; Pradeep, T. The Emerging Interface of Mass Spectrometry with Materials. *NPG Asia Mater.* **2019**, *11* (1), 1–22.

(2) Antoine, R. Supramolecular Gold Chemistry: From Atomically Precise Thiolate-Protected Gold Nanoclusters to Gold-Thiolate Nanostructures. Nanomaterials **2020**, 10 (2), 377.

(3) Zerbino, C.; Chirot, F.; Dugourd, P.; Antoine, R. The Emergence of Mass Spectrometry for Characterizing Nanomaterials. Atomically Precise Nanoclusters and Beyond. Mater. Adv., **2021**,*2, 4896-4913.*

(4) Su, P.; Hu, H.; Unsihuay, D.; Zhang, D.; Dainese, T.; Diaz, R. E.; Lee, J.; Gunaratne, D. K.; Wang, H.; Maran, F.; Mei, J.; Laskin, J. Preparative Mass Spectrometry Using a Rotating-Wall Mass Analyzer. *Angew. Chemie Int. Ed.* **2020**, *59* (20), 7711–7716.

(5) Templeton, A. C.; Wuelfing, W. P.; Murray, R. W. Monolayer-Protected Cluster Molecules. *Acc. Chem. Res.* **2000**, *33* (1), 27–36.

(6) Jin, R.; Qian, H.; Wu, Z.; Zhu, Y et al. Size Focusing: A Methodology for Synthesizing Atomically Precise Gold Nanoclusters. *J. Phys. Chem. Lett.* **2010**, *1* (19), 2903–2910.

(7) Dainese, T.; Agrachev, M.; Antonello, S.; Badocco, D. et al. Atomically Precise $Au_{144}(SR)_{60}$ Nanoclusters (R= Et, Pr) Are Capped by 12 Distinct Ligand Types of 5-Fold Equivalence and Display Gigantic Diastereotopic Effects. *Chem. Sci.* **2018**, *9* (47), 8796–8805.

(8) Dharmaratne, A. C.; Dass, A. $Au_{(144-x)}Cu_{(x)}(SC_6H_{13})_{60}$ Nanomolecules: Effect of Cu Incorporation on Composition and Plasmon-like Peak Emergence in Optical Spectra. *Chem Commun* **2014**, *50* (14), 1722–1724.

(9) Lavenn, C.; Demessence, A.; Tuel, A. Atomically Well-Defined $Au_{25}(SR)_{17/18}$ Nanoclusters Deposited on Silica Supports for the Aerobic Epoxidation of Trans-Stilbene. *Catal. Today* **2014**, *235*, 72–78.

(10) Qian, H.; Zhu, Y.; Jin, R. Atomically Precise Gold Nanocrystal Molecules with Surface Plasmon Resonance. *Proc. Natl. Acad. Sci.* **2012**, *109* (3), 696–700.

(11) Jin, R.; Zeng, C.; Zhou, M.; Chen, Y. Atomically Precise Colloidal Metal Nanoclusters and Nanoparticles: Fundamentals and Opportunities. *Chem. Rev.* **2016**, *116* (18), 10346–10413.

(12) Chakraborty, I.; Pradeep, T. Atomically Precise Clusters of Noble Metals: Emerging Link between Atoms and Nanoparticles. *Chem. Rev.* **2017**, *117* (12), 8208–8271.

(13) Eswaramoorthy, S. K.; Sakthivel, N. A.; Dass, A. Core Size Conversion of Au_{329} $(SCH_2CH_2Ph)_{84}$ to $Au_{279}(SPh\text{-}t\ Bu)_{84}$ Nanomolecules. *J. Phys. Chem. C* **2019**, *123* (14), 9634–9639.

(14) Dainese, T.; Antonello, S.; Bonacchi, S.; Morales-Martinez, D. et al. Isolation of the $Au_{145}(SR)_{60}X$ Compound (R = n-Butyl, n-Pentyl; X = Br, Cl): Novel Gold Nanoclusters That Exhibit Properties Subtly Distinct from the Ubiquitous Icosahedral $Au_{144}(SR)_{60}$ Compound. *Nanoscale* **2021**, *13* (36), 15394–15402.

(15) Black, D. M.; Bhattarai, N.; Bach, S. B. H.; Whetten, R. L. Selection and Identification of Molecular Gold Clusters at the Nano(Gram) Scale: Reversed Phase HPLC–ESI–MS of a Mixture of Au-Peth MPCs. *J. Phys. Chem. Lett.* **2016**, *7* (16), 3199–3205.

(16) Chaki, N. K.; Negishi, Y.; Tsunoyama, H.; Shichibu, Y.; Tsukuda, T. Ubiquitous 8 and 29 KDa Gold:Alkanethiolate Cluster Compounds: Mass-Spectrometric Determination of Molecular Formulas and Structural Implications. *J. Am. Chem. Soc.* **2008**, *130* (27), 8608–8610.

(17) Fields-Zinna, C. A.; Sardar, R.; Beasley, C. A.; Murray, R. W. Electrospray Ionization Mass Spectrometry of Intrinsically Cationized Nanoparticles, $[Au_{144/146}\ (SC_{11}H_{22}N\ (CH_2CH_3)_3^+)_x\ (S(CH_2)_5CH_3)_y]^{X+}$. *J. Am. Chem. Soc.* **2009**, *131* (44), 16266–16271.

(18) Black, D. M.; Hoque, M. M.; Placencia-Villa, G.; Whetten, R. L. New Evidence of the Bidentate Binding Mode in 3-MBA Protected Gold Clusters: Analysis of Aqueous 13–18 Kda Gold-Thiolate Clusters by HPLC-ESI-MS Reveals Special Compositions $Au_n(3\text{-}MBA)_p$, (n = 48–67, p = 26–30). *Nanomaterials* **2019**, *9* (9), 1303.

(19) Levi-Kalisman, Y.; Jadzinsky, P. D.; Kalisman, N.; Tsunoyama, H.; Tsukuda, T.; Bushnell, D. A.; Kornberg, R. D. Synthesis and Characterization of Au_{102} (p-MBA) $_{44}$ Nanoparticles. *J. Am. Chem. Soc.* **2011**, *133* (9), 2976–2982.

(20) Bertorelle, F.; Russier-Antoine, I.; Comby-Zerbino, C.; Chirot, F. et al. Isomeric Effect of Mercaptobenzoic Acids on the Synthesis, Stability, and Optical Properties of $Au_{25}(MBA)_{18}$ Nanoclusters. *ACS omega* **2018**, *3* (11), 15635–15642.

(21) Schaaff, T. G.; Whetten, R. L. Giant Gold−Glutathione Cluster Compounds: Intense Optical Activity in Metal-Based Transitions. *J. Phys. Chem. B* **2000**, *104* (12), 2630–2641.

(22) Negishi, Y.; Nobusada, K.; Tsukuda, T. Glutathione-Protected Gold Clusters Revisited: Bridging the Gap between Gold(I)−Thiolate Complexes and Thiolate-Protected Gold Nanocrystals. *J. Am. Chem. Soc.* **2005**, *127* (14), 5261–5270.

(23) Niihori, Y.; Shima, D.; Yoshida, K.; Hamada, K. et al. High-Performance Liquid Chromatography Mass Spectrometry of Gold and Alloy Clusters Protected by Hydrophilic Thiolates. *Nanoscale* **2018**, *10* (4), 1641–1649.

(24) Zhang, B.; Wu, Z.; Cao, Y.; Yao, Q.; Xie, J. Ultrastable Hydrophilic Gold Nanoclusters Protected by Sulfonic Thiolate Ligands. *J. Phys. Chem. C* **2020** *125*(1), 489-497.

(25) Hoque, M. M.; Black, D. M.; Mayer, K. M.; Dass, A.; Whetten, R. L. Base Side of Noble Metal Clusters: Efficient Route to Captamino-Gold, $Au_n(-S(CH_2)_2N(CH_3)_2)_p$, n = 25-144. *J. Phys. Chem. Lett.* **2019**, *10* (12), 3307–3311.

(26) Hoque, M. M.; Dass, A.; Mayer, K. M.; Whetten, R. L. Protein-Like Large Gold Clusters Based on the ω-Aminothiolate DMAET: Precision Thermal and Reaction Control Leading to Selective Formation of Cationic Gold Clusters in the Critical Size Range, n = 130-144 Gold Atoms. *J. Phys. Chem. C* **2019**, *123* (23), 14871–14879.

(27) Narita, K.; Ishida, Y.; Yonezawa, T.; Huang, Z. Super Polycationic Molecular Compounds: $Au_{144}(SR^+)_{60}$ Clusters. *J. Phys. Chem. C* **2019**, *123* (35), 21768–21773.

(28) Black, D. M.; Robles, G.; Lopez, P.; Bach, S. B. H. et al. Liquid Chromatography Separation and Mass Spectrometry Detection of Silver-Lipoate $Ag_{29}(LA)_{12}$ Nanoclusters: Evidence of Isomerism in the Solution Phase. *Anal. Chem.* **2018**, *90* (3), 2010–2017.

(29) Lopez, P.; Lara, H. H.; M. Mullins, S.; M. Black, D. et al. Tetrahedral (T) Closed-Shell Cluster of 29 Silver Atoms & 12 Lipoate Ligands, $[Ag_{29}(R\text{-}\alpha\text{-}LA)_{12}]^{(3-)}$: Antibacterial and Antifungal Activity. *ACS Appl. Nano Mater.* **2018**, *1* (4), 1595–1602.

(30) Whetten, R. L.; Weissker, H.-C.; Pelayo, J. J.; Mullins, S. M.; López-Lozano, X.; Garzón, I. L. Chiral-Icosahedral (I) Symmetry in Ubiquitous Metallic Cluster Compounds (145A,60X): Structure and Bonding Principles. *Acc. Chem. Res.* **2019**, *52* (1), 34–43.

(31) Tran, N. T.; Powell, D. R.; Dahl, L. F. Nanosized $Pd_{145}(CO)_x$ $(PEt3)_{30}$ Containing a Capped Three-Shell 145-Atom Metal-Core Geometry of Pseudo Icosahedral Symmetry. *Angew. Chemie Int. Ed.* **2000**, *39* (22), 4121–4125.

(32) Yan, N.; Xia, N.; Liao, L.; Zhu, M.; Jin, F.; Jin, R.; Wu, Z. Unraveling the Long-Pursued Au144 Structure by x-Ray Crystallography. Sci. Adv. 2023, 4 (10), eaat7259

(33) Hong, R.; Emrick, T.; Rotello, V. M. Monolayer-Controlled Substrate Selectivity Using Noncovalent Enzyme−Nanoparticle Conjugates. *J. Am. Chem. Soc.* **2004**, *126* (42), 13572–13573.

(34) Zhu, Z.-J.; Ghosh, P. S.; Miranda, O. R.; Vachet, R. W.; Rotello, V. M. Multiplexed Screening of Cellular Uptake of Gold Nanoparticles Using Laser Desorption/Ionization Mass Spectrometry. *J. Am. Chem. Soc.* **2008**, *130* (43), 14139–14143.

(35) Elci, S. G.; Jiang, Y.; Yan, B.; Kim, S. T. et al. Surface Charge Controls the Suborgan Biodistributions of Gold Nanoparticles. *ACS Nano* **2016**, *10* (5), 5536–5542.

(36) Zhu, Z.-J.; Wang, H.; Yan, B.; Zheng, H. et al. Effect of Surface Charge on the Uptake and Distribution of Gold Nanoparticles in Four Plant Species. *Environ. Sci. Technol.* **2012**, *46* (22), 12391–12398.

(37) Zhu, Z.; Carboni, R.; Quercio Jr, M. J.; Yan, B. et al. Surface Properties Dictate Uptake, Distribution, Excretion, and Toxicity of Nanoparticles in Fish. *Small* **2010**, *6* (20), 2261–2265.

(38) Marsico, A. L. M.; Duncan, B.; Landis, R. F.; Tonga, G. Y.; Rotello, V. M.; Vachet, R. W. Enhanced Laser Desorption/Ionization Mass Spectrometric Detection of Biomolecules Using Gold Nanoparticles, Matrix, and the Coffee Ring Effect. *Anal. Chem.* **2017**, *89* (5), 3009–3014.

(39) Marsico, A. L. M.; Elci, G. S.; Moyano, D. F.; Yesilbag Tonga, G. et al. Enhanced Laser Desorption/Ionization Mass Spectrometric Detection of Gold Nanoparticles in Biological Samples Using the Synergy between Added Matrix and the Gold Core. *Anal. Chem.* **2015**, *87* (24), 12145–12150.

(40) Ruotolo, B. T.; Benesch, J. L. P.; Sandercock, A. M.; Hyung, S.-J.; Robinson, C. V. Ion Mobility–Mass Spectrometry Analysis of Large Protein Complexes. *Nat. Protoc.* **2008**, *3* (7), 1139–1152.

(41) Seto, S.; Takeda, T.; Hoshino, N.; Akutagawa, T. Effective Na+-Binding Ability and Molecular Assembly of an Alkylamide-Substituted Penta(Ethylene)Glycol Derivative. J. Phys. Chem. B **2021**, *125* (23), 6349–6358.

(42) Ruotolo, B. T.; Benesch, J. L. P.; Sandercock, A. M.; Hyung, S.-J.; Robinson, C. V. Ion Mobility–Mass Spectrometry Analysis of Large Protein Complexes. Nat. Protoc. **2008**, *3* (7), 1139–1152

(43) Rostom, A. A.; Robinson, C. V. Detection of the Intact GroEL Chaperonin Assembly by Mass Spectrometry. *J. Am. Chem. Soc.* **1999**, *121* (19), 4718-4719.

(44) Vis, H.; Heinemann, U.; Dobson, C. M.; Robinson, C. V. Detection of a Monomeric Intermediate Associated with Dimerization of Protein Hu by Mass Spectrometry. *J. Am. Chem. Soc.* **1998**, *120* (25), 6427-6428.

(45) McCammon, M. G.; Hernández, H.; Sobott, F.; Robinson, C. V. Tandem Mass Spectrometry Defines the Stoichiometry and Quaternary Structural Arrangement of Tryptophan Molecules in the Multiprotein Complex TRAP. *J. Am. Chem. Soc.* **2004**, *126* (19), 5950–5951.